

Relativistic electron precipitation by EMIC waves: importance of nonlinear resonant effects

Veronika S. Grach¹, Anton V. Artemyev^{2,3}, Andrei G. Demekhov^{1,4},
Xiao-Jia Zhang², Jacob Bortnik², Vassilis Angelopoulos², R. Nakamura⁵, E.
Tsai², C. Wilkins², O. W. Roberts⁵

¹Institute of Applied Physics, Russian Academy of Sciences, Nizhny Novgorod, Russia

²University of California, Los Angeles, Los Angeles, USA

³Space Research Institute RAS, Moscow, Russia.

⁴Polar Geophysical Institute, Apatity, Russia

⁵Space Research Institute, Austrian Academy of Science, Graz, Austria

Key Points:

- ELFIN observations of EMIC-driven precipitation of relativistic electrons
- Test-particle model reproduce precipitating electron energy range
- Nonlinear resonant effects cannot stop the diffusive scattering into loss-cone

arXiv:2205.00515v1 [physics.space-ph] 1 May 2022

Corresponding author: Veronika S. Grach, vsgrach@ipfran.ru

Abstract

Relativistic electron losses in Earth’s radiation belts are usually attributed to electron resonant scattering by electromagnetic waves. One of the most important wave mode for such scattering is the electromagnetic ion cyclotron (EMIC) mode. Within the quasi-linear diffusion framework, the cyclotron resonance of relativistic electrons with EMIC waves results in very fast electron precipitation to the atmosphere. However, wave intensities often exceed the threshold for nonlinear resonant interaction, and such intense EMIC waves have been shown to transport electrons away from the loss cone due to the *force bunching* effect. In this study we investigate if this transport can block electron precipitation. We combine test particle simulations, low-altitude ELFIN observations of EMIC-driven electron precipitation, and ground-based EMIC observations. Comparing simulations and observations, we show that, despite of the low pitch-angle electrons being transported away from the loss cone, the scattering at higher pitch angles results in the loss cone filling and electron precipitation.

1 Introduction

Dynamics of relativistic electron fluxes in the Earth’s inner magnetosphere is largely controlled by the competition of acceleration processes (due to resonances with whistler-mode waves and/or radial transport, see, e.g., Shprits, Subbotin, et al., 2008; Shprits, Elkington, et al., 2008; Millan & Baker, 2012, and references therein) and losses, which are significantly contributed by electron resonant interaction with electromagnetic ion cyclotron (EMIC) waves (see, e.g., Usanova et al., 2014; Ma et al., 2015; Drozdov et al., 2017). EMIC waves are generally much stronger than whistler-mode waves, and the resulted relativistic electron scattering can be incredibly fast (see estimates of EMIC-driven diffusion rates in Summers & Thorne, 2003; Kersten et al., 2014; Ni et al., 2015; Shprits et al., 2016). The main approach to quantify the EMIC-driven electron losses in the radiation belt models is the quasi-linear theory (e.g., Thorne & Kennel, 1971; Albert, 2003; Glauert & Horne, 2005), which operates with diffusion rates calculated under the assumption of weak wave intensity (Vedenov et al., 1962; Drummond & Pines, 1962; Andronov & Trakhtengerts, 1964; Kennel & Petschek, 1966). Spacecraft observations, however, often show EMIC wave intensities sufficiently large to exceed the threshold of quasi-linear diffusion applicability (see discussion in Wang et al., 2017; Grach et al., 2021). Therefore, an important question in modeling relativistic electron losses is how does electron scattering change for intense EMIC waves?

In contrast to diffusion by low amplitude waves, intense waves resonate with electron nonlinearly. Such nonlinear resonant interaction includes phase trapping and phase bunching, which provide direct transport of electrons in pitch-angle space (see reviews by Karpman, 1974; Omura et al., 1991; Shklyar & Matsumoto, 2009; Albert et al., 2013; Artemyev et al., 2018). For relativistic electron resonances with EMIC waves, phase bunching results in electron transport away from the loss cone (Albert & Bortnik, 2009), whereas phase trapping quickly moves electrons into the loss cone and may result in strong precipitation (Omura & Zhao, 2013; Kubota et al., 2015; Kubota & Omura, 2017). Moreover, in low pitch angles (close to the loss cone), the nonlinear wave-particle interaction is significantly modified (see, e.g., Kitahara & Katoh, 2019; Albert et al., 2021; Artemyev, Neishtadt, et al., 2021), which is particularly important for relativistic electron resonances with EMIC waves but not included in most existing models. Around the loss cone, EMIC wave interaction with electrons does not include phase trapping but is dominated by the so-called force bunching effect (Grach & Demekhov, 2020), which leads to rapid pitch-angle increases. Such direct transport away from the loss cone may block the electron precipitation (see discussion in Bortnik et al., 2022). Thus, it remains paradoxical where increased EMIC wave amplitude above

the threshold of nonlinear resonant interaction may result in decreased efficiency of electron scattering into loss cone.

In this case study we focus on detailed investigation of relativistic electron scattering by intense EMIC waves. We use electron precipitation observations at low-altitude ELFIN CubeSats (Angelopoulos et al., 2020) and conjugate EMIC wave observations at the Lovozero ground-based station (Fedorenko et al., 2014). We also use measurements from the Magnetospheric Multiscale (MMS) mission (Burch et al., 2016) to probe the equatorial plasma conditions important for electron resonances with EMIC waves (see Summers, 2005; Summers et al., 2007). Spacecraft and ground-based measurements are combined with test particle simulations that include realistic models of EMIC wave propagation (see Grach et al., 2021). We show that the force phase bunching indeed quickly moves relativistic electrons to higher pitch angles, but EMIC waves also scatter high pitch-angle electrons directly into loss cone. The competition of these two processes results in loss-cone filling and electron precipitation observed by ELFIN. The paper is structured as follows: descriptions of spacecraft and ground-based observations in Section 2, discussion of test particle simulation results in Section 3, and conclusions in Section 4.

2 Spacecraft observations

Figure 1 shows the event overview with ELFIN observations of EMIC-driven electron precipitation. Energetic particle detector (EPDe) onboard ELFIN measures electrons in the [50, 7000] keV energy range (16 channels, $\Delta E/E \approx 0.4$) and $\in [0, 360^\circ]$ pitch-angle range (16 sectors, $\Delta\alpha = 22.5^\circ$) with a 1.5 s (half spin) resolution (Angelopoulos et al., 2020). Panel (a) shows the energy spectrum of trapped electrons (pitch angle $\alpha \in [\alpha_{LC}, 180^\circ - \alpha_{LC}]$, where α_{LC} is the local loss-cone angle). ELFIN moved from low L -shells to higher L -shells on the dusk flank (see panel (d)), along which ELFIN traversed the plasmasphere (according to equatorial spacecraft measurements, the plasmopause is located around $L(T89) \sim 6$, see discussion below) and outer radiation belt. Around the plasmopause, at 13:21:05 UT, trapped electron fluxes of relativistic energies (> 700 keV) show a local maximum. Note that the locally trapped electrons at ELFIN map to small equatorial pitch angles, right outside the equatorial loss cone. Such transient flux increases shall be interpreted as a spatially localized enhancement of small pitch-angle electron fluxes at the equator. Panels (b,c) confirm that increases of trapped fluxes are accompanied by strong precipitation of relativistic electrons. There are two important features of this transient precipitation: First, precipitating fluxes and ratio of precipitating-to-trapped fluxes maximize at relativistic energies (> 700 keV) without a significant precipitation of < 500 keV electrons, which would indicate electron scattering by whistler-mode waves (compare the precipitation at 13:21:05 UT and precipitation likely driven by plasmaspheric hiss at 13:20:35-13:20:45 UT; also see the discussion of ELFIN observations of whistler-mode wave driven precipitation in Mourenas et al. (2021); Artemyev, Demekhov, et al. (2021)); Second, precipitating fluxes at relativistic energies (around ~ 1 MeV) almost reach the strong diffusion limit (see the comparison of precipitating and trapped electron spectra in panel (e)). These two features strongly suggest that the observed precipitation is driven by electron scattering by EMIC waves (see similar equatorial observations of small pitch-angle flux enhancements associated with EMIC waves in Zhu et al., 2020), which resonate with relativistic electrons most effectively (Albert, 2003; Kersten et al., 2014; Ni et al., 2015; Shprits et al., 2017) and are well able to cause precipitation in the strong diffusion limit (Omura & Zhao, 2013; Kubota & Omura, 2017; Grach & Demekhov, 2020). Panels (b,e) show that in addition to the clear precipitation peak at ~ 1 MeV, there exists moderate precipitation down to 50 keV. Such weak electron precipitation at lower energies may be attributed to electron scattering by whistler-mode hiss

waves around the plasmasphere (see discussion of hiss wave localization around the plasmasphere in, e.g., Malaspina et al., 2020).

Figure 2(a) shows that the ELFIN orbit with EMIC-driven electron precipitation is projected nearby the ground-based magnetometer station (LOZ), whereas the same (*MLT*, *L*-shell) region was traversed by MMS spacecraft ~ 1.5 hours later. Due to the time difference between MMS and ELFIN crossings of $L \in [6, 7]$, field-aligned helium band EMIC waves detected by MMS (see panels (b,c)) cannot be directly associated with the precipitation at ELFIN (although the EMIC wave source region may survive for several hours, see Engebretson et al., 2015). Note that MMS were at middle latitudes, well below the equator, and hence cannot detect all near-equatorial EMIC waves that possibly persist after $\sim 14:00$ UT.

We use spacecraft potential measurements (Ergun et al., 2016; Lindqvist et al., 2016; Torkar et al., 2014) and the inner magnetosphere temperature model (Boardsen et al., 2014) to estimate the cold plasma density at MMS (Andriopoulou et al., 2016, 2018). Figure 2(d) shows plasma density enhancements around the plasmopause, at $L \in [8, 6]$, with the peak density reaching $\sim 40 \text{ cm}^{-3}$. Such density enhancements can survive for hours (e.g., Goldstein et al., 2014), which can then guide EMIC wave propagation to the ionosphere. Indeed, the LOZ station detected frequency-banded, $\in [0.2, 1] \text{ Hz}$, waves resembling properties of EMIC emissions measured by MMS (see panel (e)). More importantly, ground-based observations of EMIC waves are in a good conjunction with ELFIN precipitation measurements. Therefore, we may assume that the precipitation at ELFIN is driven by helium band EMIC waves, whereas localized plasma density peaks reduce the electron resonant energies to $\sim 1 \text{ MeV}$, as shown in the precipitation energy at ELFIN.

3 Simulation setup and results

To investigate the mechanism of electron precipitation observed by ELFIN, we perform a test particle simulation with observed EMIC wave characteristics. We use the dipole model of geomagnetic field \mathbf{B}_0 and gyrotropic model of plasma density $N = N_{eq}B_0/B_{0eq}$, where the subscript "eq" denotes equatorial values. Based on MMS measurements (see Fig. 2(d)), we choose $L = 6.2$, $N_{eq} = 40 \text{ cm}^{-3}$, and use the plasmaspheric ion composition $N_{H^+} = 0.8N$, $N_{He^+} = 0.2N$ from Horwitz et al. (1990). Wave packet parameters (constant wave frequency $f = 0.95f_{He^+} = 0.48 \text{ Hz}$ and duration $\tau = 120 \text{ s}$) are set in agreement with ground-based (LOZ) observations; here f_{He^+} is helium gyrofrequency. We also assume a Gaussian amplitude profile with the maximum wave amplitude $B_{wm} = 2 \text{ nT}$.

EMIC wave packet is generated in a small region near the equator and then propagates along the magnetic field lines. The spatial-temporal distribution of the wave field is retrieved using the ray-tracing technique, as shown in Figure 3(a) (see also the distribution zoomed around the equator in panel (b)). In ray-tracing, the wave energy flux $\mathcal{E} \propto B_w^2 V_{gr}/(8\pi)$ for each point of the packet remains constant, and the group velocity V_{gr} corresponds to the local wave dispersion relation (see details of wave model in Grach et al., 2021).

The model wave field is then used to evaluate trajectories of test electrons interacting with EMIC waves at the anomalous cyclotron resonance. We use the gyro-averaged electron equations of motion (see details in Grach & Demekhov, 2020; Grach et al., 2021):

$$\frac{dW}{dt} = -ev_{\perp}|E_w| \sin \Psi; \quad (1)$$

$$\frac{dI_{\perp}}{dt} = -\frac{2e}{mB_0}p_{\perp}(1 - n_{||}\beta_{||})|E_w| \sin \Psi; \quad (2)$$

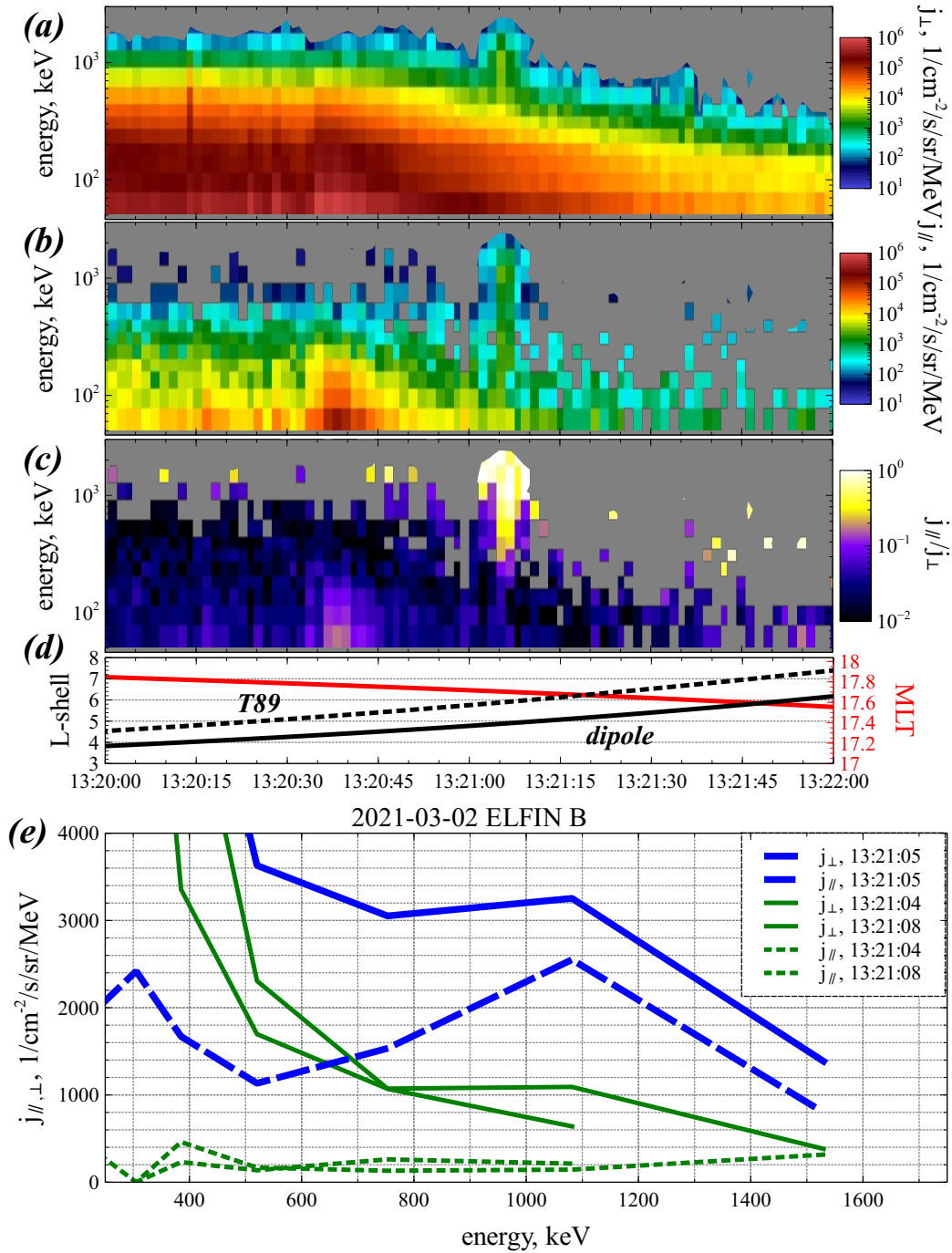


Figure 1. An overview of ELFIN B observations on 2 March 2021: energy spectrum of trapped electron fluxes (a), spectrum of precipitating electron fluxes (b), precipitating-to-trapped flux ratio (c), ELFIN B MLT and L -shell calculated with the dipole and (Tsyganenko, 1989) magnetic field models (d), spectra of trapped (\perp) and precipitating (\parallel) fluxes around the precipitation burst (e).

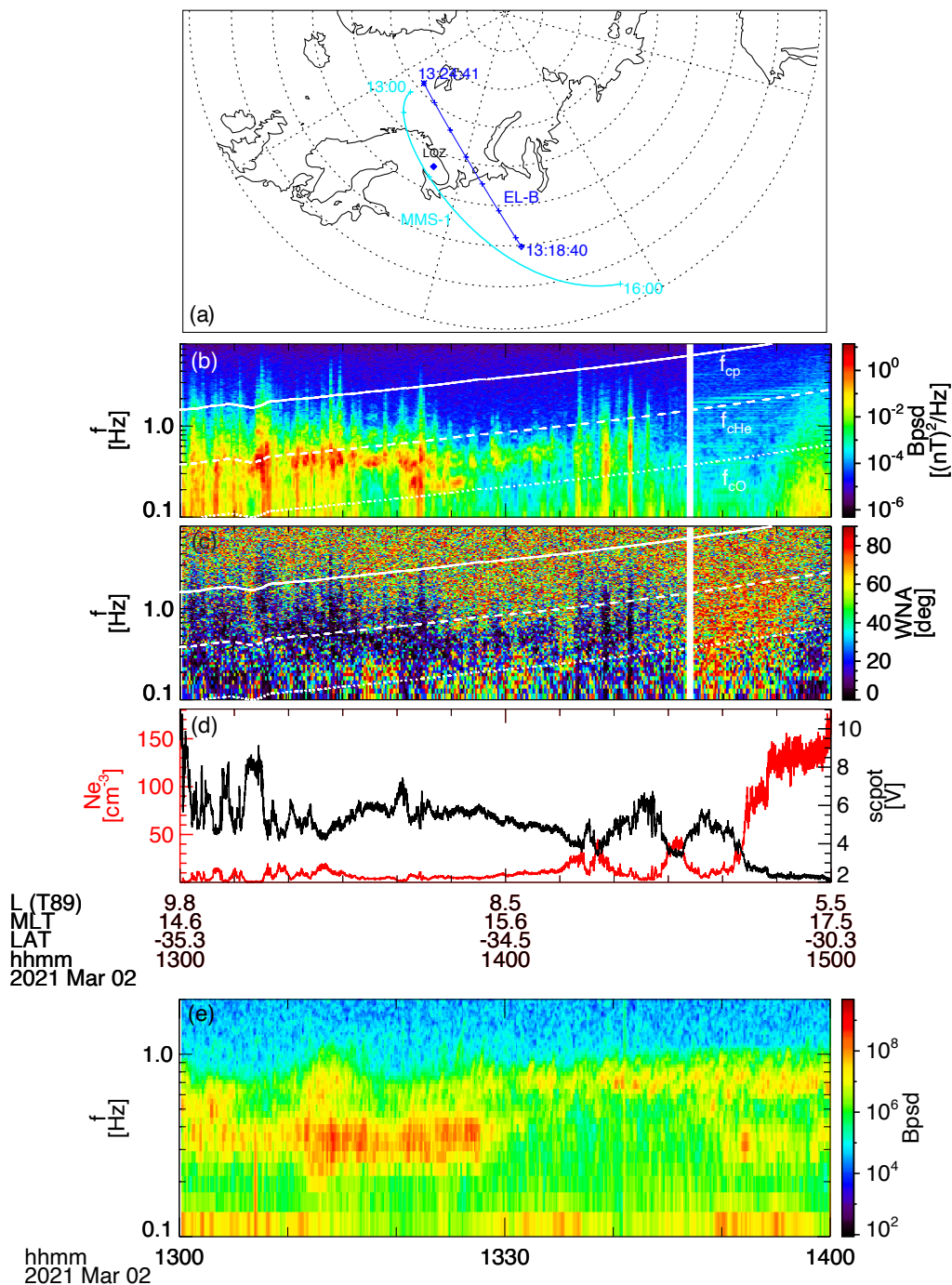


Figure 2. Overview of EMIC wave measurements: projections of ELFIN B and MMS #1 orbits to the northern hemisphere with the ground-based LOZ station (a), MMS magnetic field spectrum in the EMIC wave frequency range (b), EMIC wave normal angle distributions (c), MMS spacecraft potential and the inferred density (d), spectrum of EMIC wave magnetic field measured at the LOZ station (e).

$$\frac{d\Psi}{dt} = -\Delta - \frac{e}{p_{\perp}}(1 - n_{\parallel}\beta_{\parallel})|E_w| \cos \Psi; \quad (3)$$

$$\frac{dz}{dt} = \frac{p_{\parallel}}{m\gamma}. \quad (4)$$

Here subscripts \parallel and \perp denote projections to the parallel and transverse directions with respect to \mathbf{B}_0 ; $W = (\gamma - 1)mc^2$ and $I_{\perp} = p_{\perp}^2/(mB_0)$ are the electron kinetic energy and the first adiabatic invariant; $\gamma = \sqrt{1 + [p/(mc)]^2}$ is the Lorentz factor; m , p and v are the electron rest mass, momentum, and velocity; $\beta_{\parallel} = v_{\parallel}/c$, $n_{\parallel} = kc/\omega$; $\omega = 2\pi f$, k and E_w are wave frequency, wave number, and slowly changing wave electric field amplitude; z is the coordinate along the geomagnetic field with $z = 0$ corresponding to the equator; $\Psi = \vartheta - \varphi$, φ is the gyrophase in the geomagnetic field \mathbf{B}_0 ; $\vartheta = \omega/c \int n_{\parallel} dz - \int \omega dt$ is the wave phase, $\Delta = \omega - kv_{\parallel} + \Omega_c/\gamma$ is the mismatch from the resonance; $\Omega_c = eB_0/mc$, with $e > 0$ being the elementary charge.

These equations of motion (1)–(4) are solved numerically by Bogacky-Shampine variant of the Runge-Kutta method. We use $\sim 0.5 \cdot 10^6$ trajectories with 19 initial energies $W_0 \in [0.5, 2.0]$ MeV, 135 initial equatorial pitch angles $\alpha_{eq0} \in [3^\circ, 70^\circ]$, and 180 initial phases uniformly distributed in $[0, 2\pi)$. Note that for the considered L , the loss-cone angle is $\alpha_{eq}^{LC} \approx 2.7^\circ$. To investigate variations of electron scattering as the wave packet evolves along magnetic field lines (see Fig. 3(a,b)), we run three simulations where the electron trajectories start from the equator at times $t_S = 130, 220$, and 300 s, respectively. Electron energy remains nearly constant during the resonant interaction with EMIC waves (because the wave frequency is much smaller than electron gyrofrequency), and hence we characterize the resonant interaction by the change of equatorial pitch angles, α_{eq} . We calculate the mean electron pitch angle change $\langle \Delta\alpha_{eq} \rangle$ and spread $\sigma_{\alpha} = \sqrt{\langle (\Delta\alpha_{eq})^2 \rangle - \langle \Delta\alpha_{eq} \rangle^2}$ as functions of initial energy and pitch angle.

Figure 3(c,d) shows $\langle \Delta\alpha_{eq} \rangle$, σ_{α} maps for three different test particle runs (i.e., three different wave field distributions at the resonant latitudes). Electrons with small initial pitch angles show a significant $\langle \Delta\alpha_{eq} \rangle > 0$ at the resonant energy that increases with time (with the resonant latitudes where the wave-packet intensity maximises) from 1 MeV to 1.5 MeV (see red regions in Figure 3(c)). Such a pitch-angle *reflection* from the loss cone has been found by (Lundin & Shkliar, 1977; Inan et al., 1978) and described for EMIC waves in Grach and Demekhov (2020) as *force phase bunching*. This pitch-angle change is described by the second term of the right-hand side of Eq. (3): the direct influence of Lorentz force on the particle phase is strong for small p_{\perp} and can exceed the inertial (or kinematic) bunching effect of the the first term in Eq. (3). Figure 3(e) shows this force phase bunching with pitch-angle increase in test trajectories (see also statistical investigation of this effect in Bortnik et al., 2022).

For electrons with pitch angles exceeding $\sim 10^\circ$, the resonant interaction with EMIC waves results in predominantly $\langle \Delta\alpha_{eq} \rangle < 0$ (see blue stripes in Fig. 3(c)). However, this electron drift toward the loss cone is not very strong ($\langle \Delta\alpha_{eq} \rangle > -5^\circ$), because the corresponding initial energies/pitch angles are outside the domain of resonant interactions (shown by black curves). For $\alpha_{eq} > 10^\circ$ within the resonant domain, the pitch-angle drift is almost absent, $\langle \Delta\alpha_{eq} \rangle \approx 0$. Spread in pitch-angle scattering, however, is quite large for $\alpha_{eq} > 10^\circ$ electrons: $\sigma_{\alpha} > 5^\circ$ (see Fig. 3(d)). Several test particle trajectories in Fig. 3(f) shows that such diffusive scattering (almost symmetric in the number of particles with $\Delta\alpha_{eq} > 0$ and $\Delta\alpha_{eq} < 0$) may move 10° – 15° electrons directly into the loss cone, and these electrons should move to the atmosphere after a single resonant interaction. Note that in the considered case of relatively strong wave amplitude and short packet duration, the resonant interaction zone is determined by the packet length (see Figures 3e,f and resonant range in Figures 3c,d). This situation is quite common for realistic EMIC wave packets (Grach & Demekhov, 2020; Grach et al., 2021).

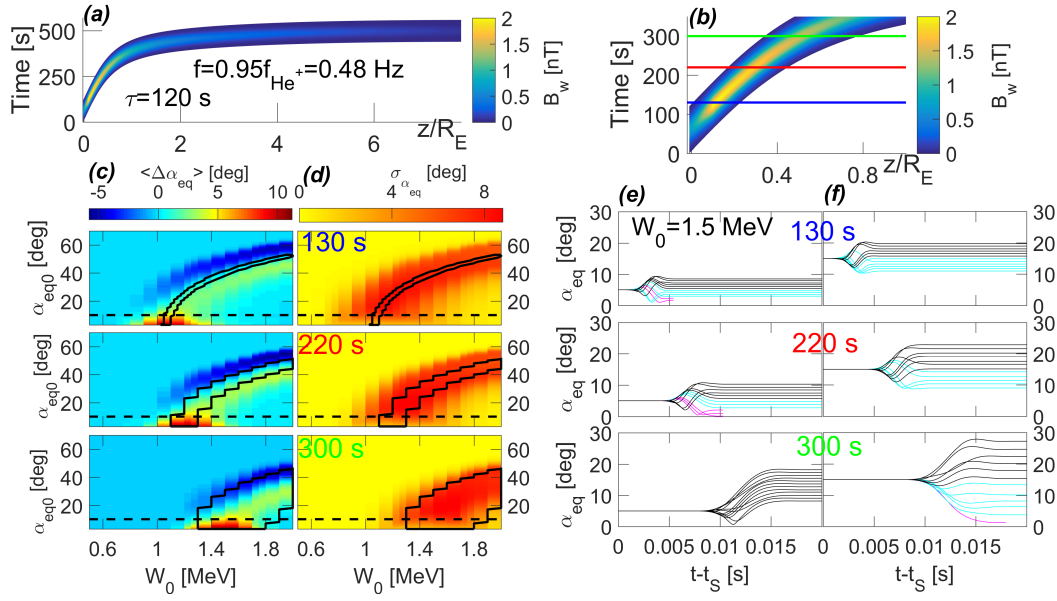


Figure 3. (a-b): The spatial-temporal distribution of EMIC wave field as the wave packet propagates away from its source region near the equator ($z=0$). Horizontal lines in (b) mark the start times (t_S) of electron trajectories in three runs. (c-d): Phase averaged change in α_{eq} and rms $\sigma_{\alpha_{eq}}$ after a single pass through the wave packet at times t_S as a function of initial energy W_0 and equatorial pitch angle α_{eq0} . Black contours show unperturbed resonant domains (where the exact resonance condition with $\Delta = 0$ is satisfied); dashed lines correspond to $\alpha_{eq0} = 10^\circ$. (e-f): Pitch-angle trajectories for particles with $W_0 = 1.5$ MeV and $\alpha_{eq0} = 5^\circ, 15^\circ$. Black, cyan, and magenta lines correspond, respectively, to those with pitch-angle increasing and decreasing, and particles scattered into the loss cone.

To investigate effects of electron scattering by EMIC waves on electron dynamics, we follow the approach proposed in (Grach & Demekhov, 2020; Grach et al., 2021). Assigning each test particle a specific weight, we specify an initial pitch angle distribution $\Phi_{\alpha_{eq}}^{(0)}$ (uniform in our case) and calculate the distribution function $\Phi_{\alpha_{eq}}$ after the wave-particle interactions. The normalized distribution $\tilde{\Phi} = \Phi_{\alpha_{eq}}/\Phi_{\alpha_{eq}}^{(0)}$ is shown in Figure 4a. The loss cone (the smallest pitch-angle bin) is empty at the beginning, but becomes filled by electrons scattered by EMIC waves. Note that the energy range of the loss-cone filling changes with time because different energies resonate with EMIC wave-packet at different latitudes (at different times).

Figure 4b shows the percentage of particles (in each pitch-angle/energy bin) that increase their pitch angles during the simulation. This distribution mainly repeats $\langle \Delta\alpha_{eq} \rangle$ distribution from Fig. 3c. Almost all resonant electrons with small initial pitch angles move away from the loss cone ($\delta N_{p+} \approx 100\%$). Resonant electrons with pitch angles above 10° are scattered in a diffusive way: about half electron populations increase pitch angles ($\delta N_{p+} \approx 50\%$) and the other half decrease pitch angles.

Figure 4c shows distribution of percentage of electrons that are scattered directly into the loss cone after a single resonant interaction with EMIC waves. For the main energy range of resonance, a population of $> 5^\circ$ electrons ($\sim 10\%$ of total electron population) are scattered into the loss cone. Such electrons have initial pitch angles sufficiently large to avoid the positive drift away from the loss cone (compare Figs. 3c and 4c), i.e., electrons can jump over the small pitch-angle range with $\langle \Delta\alpha_{eq} \rangle > 0$ and move directly into the loss cone.

To compare simulation results with ELFIN data, we plot the ratio of the precipitating flux and flux of trapped particles with equatorial pitch angles of $[\alpha_{eq}^{LC}, \alpha_{eq}^{LC} + 5^\circ]$. Figure 4d shows this ratio (solid curve) as a function of energy for three time moments. The energy range $[0.8, 1.8]$ MeV corresponds to very strong precipitation on the strong diffusion limit (with precipitating fluxes reaching the trapped flux level). Comparison of Fig. 4d and Figs. 1c,e confirms that simulation reproduces the observed energies of strong precipitation.

We also analyzed the effects of long-term interactions, for which we run three simulations in the time interval of $[t_S - 2.5 \text{ s}, t_S + 2.5 \text{ s}]$, corresponding to 6 – 12 bounce oscillations for electrons with energies of 0.5 to 2 MeV. On this time scale, wave packet evolution is insignificant, so temporal dynamics is determined by the particle redistribution over pitch angles. Time averaged precipitating flux is roughly the same as in the case of the single interaction, but there are also transient bursts of precipitation deviating from the averaged level. For illustration, the maximum ratio $j_{||}/j_{\perp}$ is shown in Figure 4d as dotted lines. One can see that in some cases precipitating flux can be twice as high as the trapped flux.

4 Discussion and Conclusions

This study is focused on a detailed investigation of EMIC-driven relativistic electron precipitation as observed by ELFIN CubeSats and reproduced in numerical simulations. We aim to examine the effect of electron force phase bunching that moves small pitch-angle electrons away from the loss cone and may potentially block their precipitation (see Bortnik et al., 2022). Observationally driven test particle simulations show that although the force phase bunching indeed prevents precipitation of $\alpha_{eq} < 10^\circ$ electrons, electrons with $\alpha_{eq} > 10^\circ$ can still be efficiently scattered towards small pitch angles. Such a scattering may move $\alpha_{eq} > 10^\circ$ electrons directly into the loss cone, and these electrons will be precipitated without having a chance to be transported away from the loss cone by the force phase bunching effect. Precipitating

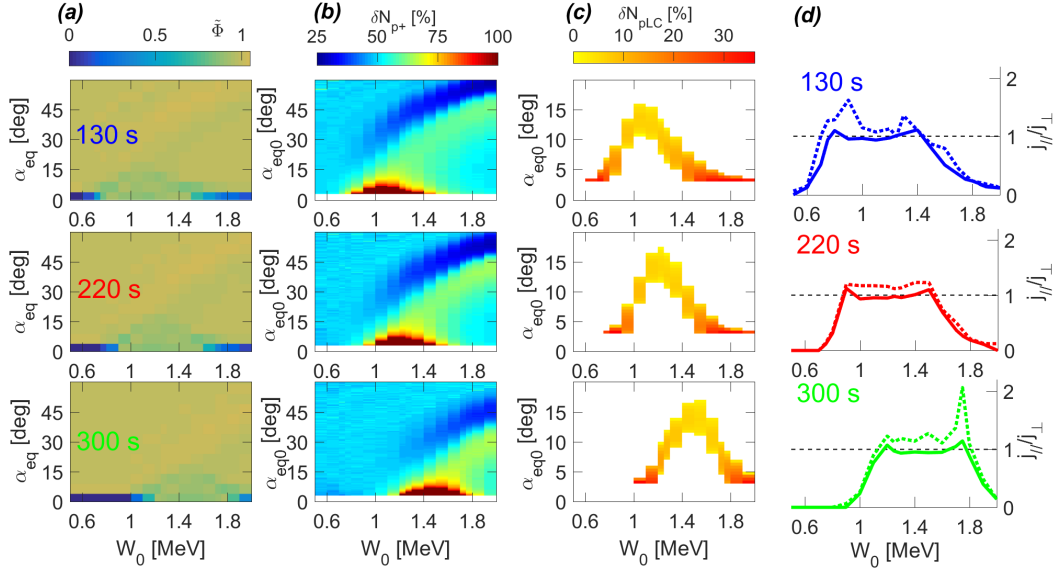


Figure 4. Distribution of the particle ensemble after a single pass through the wave packet. Top, middle, and bottom rows correspond to start times of 130, 220, and 300 s, respectively. (a): Pitch-angle distribution; (b) and (c): the fraction of particles with increased pitch angles and scattered into the loss cone, respectively; (d) the ratio between the precipitating flux and the flux of trapped particles with $\alpha_{eq}^{LC} \leq \alpha_{eq} < \alpha_{eq}^{LC} + 5^\circ$ (solid line). Dotted lines in column (d) show the maximum ratio of the precipitating and trapped fluxes during the 5-second simulation.

electron measurements at low altitudes by ELFIN confirm the strong precipitation within the energy range of expectation from simulations.

Therefore, the main conclusion of this study is that the force phase bunching cannot completely prevent precipitation, but may change the pitch-angle range of precipitating electrons. This nonlinear effect should influence the electron pitch-angle distributions in association with EMIC waves, as measured by near-equatorial spacecraft (e.g., Bingley et al., 2019; Zhu et al., 2020), but can unlikely change the strong precipitating rate provided by EMIC waves in radiation belt models. Therefore, the force phase bunching must be taken into account for short-term simulations and interpretation of observations of EMIC-driven electron precipitation bursts, but may have a secondary importance for long-term simulations of radiation belt dynamics.

Acknowledgments

We are grateful to NASA’s CubeSat Launch Initiative for ELFIN’s successful launch in the desired orbits. We acknowledge early support of ELFIN project by the AFOSR, under its University Nanosat Program, UNP-8 project, contract FA9453-12-D-0285, and by the California Space Grant program. We acknowledge critical contributions of numerous volunteer ELFIN team student members. We appreciate the access to LOZ Pc1 data (PI: Yury Fedorenko). X.-J. Z. acknowledges support from the NSF grant 2021749. V.S.G. acknowledges support from RSF grant 19-72-10111 (numerical simulations in Section 3). A.V.A, X.-J.Z., and J.B. acknowledge support from the NASA grant 80NSSC20K1270. Analysis of the spacecraft potential data at IWF (R.N. and O. W. R.) is supported by Austrian FFG Project No. ASAP15/873685

Open Research

ELFIN data is available at <https://data.elfin.ucla.edu/>.

MMS data is available at <https://lasp.colorado.edu/mms>.

LOZ data is available at <http://aurora.pgia.ru:8071/>.

Data analysis was done using SPEDAS V4.1 (Angelopoulos et al., 2019) available at <https://spedas.org/>.

References

- Albert, J. M. (2003, Jun). Evaluation of quasi-linear diffusion coefficients for EMIC waves in a multispecies plasma. *Journal of Geophysical Research (Space Physics)*, *108*(A6), 1249. doi: 10.1029/2002JA009792
- Albert, J. M., Artemyev, A. V., Li, W., Gan, L., & Ma, Q. (2021). Models of resonant wave-particle interactions. *Journal of Geophysical Research: Space Physics*, *126*(6), e2021JA029216. doi: 10.1029/2021JA029216
- Albert, J. M., & Bortnik, J. (2009, June). Nonlinear interaction of radiation belt electrons with electromagnetic ion cyclotron waves. *Geophys. Res. Lett.*, *36*, 12110. doi: 10.1029/2009GL038904
- Albert, J. M., Tao, X., & Bortnik, J. (2013). Aspects of Nonlinear Wave-Particle Interactions. In D. Summers, I. U. Mann, D. N. Baker, & M. Schulz (Eds.), *Dynamics of the earth's radiation belts and inner magnetosphere*. doi: 10.1029/2012GM001324
- Andriopoulou, M., Nakamura, R., Torkar, K., Baumjohann, W., Torbert, R. B., Lindqvist, P.-A., ... Russell, C. T. (2016, May). Study of the spacecraft potential under active control and plasma density estimates during the MMS commissioning phase. *Geophys. Res. Lett.*, *43*, 4858-4864. doi: 10.1002/2016GL068529
- Andriopoulou, M., Nakamura, R., Wellenzohn, S., Torkar, K., Baumjohann, W., Torbert, R. B., ... Burch, J. L. (2018, April). Plasma Density Estimates From Spacecraft Potential Using MMS Observations in the Dayside Magnetosphere. *Journal of Geophysical Research (Space Physics)*, *123*(4), 2620-2629. doi: 10.1002/2017JA025086
- Andronov, A. A., & Trakhtengerts, V. Y. (1964). Kinetic instability of the Earth's outer radiation belt. *Geomagnetism and Aeronomy*, *4*, 233-242.
- Angelopoulos, V., Cruce, P., Drozdov, A., Grimes, E. W., Hatzigeorgiu, N., King, D. A., ... Schroeder, P. (2019, January). The Space Physics Environment Data Analysis System (SPEDAS). *Space Sci. Rev.*, *215*, 9. doi: 10.1007/s11214-018-0576-4
- Angelopoulos, V., Tsai, E., Bingley, L., Shaffer, C., Turner, D. L., Runov, A., ... Zhang, G. Y. (2020, July). The ELFIN Mission. *Space Sci. Rev.*, *216*(5), 103. doi: 10.1007/s11214-020-00721-7
- Artemyev, A. V., Demekhov, A. G., Zhang, X. J., Angelopoulos, V., Mourenas, D., Fedorenko, Y. V., ... Shinohara, I. (2021, November). Role of Ducting in Relativistic Electron Loss by Whistler-Mode Wave Scattering. *Journal of Geophysical Research (Space Physics)*, *126*(11), e29851. doi: 10.1029/2021JA029851
- Artemyev, A. V., Neishtadt, A. I., Albert, J. M., Gan, L., Li, W., & Ma, Q. (2021, May). Theoretical model of the nonlinear resonant interaction of whistler-mode waves and field-aligned electrons. *Physics of Plasmas*, *28*(5), 052902. doi: 10.1063/5.0046635
- Artemyev, A. V., Neishtadt, A. I., Vainchtein, D. L., Vasiliev, A. A., Vasko, I. Y., & Zelenyi, L. M. (2018, December). Trapping (capture) into resonance and scattering on resonance: Summary of results for space plasma systems. *Communications in Nonlinear Science and Numerical Simulations*, *65*, 111-160.

doi: 10.1016/j.cnsns.2018.05.004

- Bingley, L., Angelopoulos, V., Sibeck, D., Zhang, X., & Halford, A. (2019, July). The Evolution of a Pitch-Angle “Bite-Out” Scattering Signature Caused by EMIC Wave Activity: A Case Study. *Journal of Geophysical Research (Space Physics)*, *124*(7), 5042-5055. doi: 10.1029/2018JA026292
- Boardsen, S. A., Adrian, M. L., Pfaff, R., & Menietti, J. D. (2014, October). Inner magnetospheric electron temperature and spacecraft potential estimated from concurrent Polar upper hybrid frequency and relative potential measurements. *Journal of Geophysical Research (Space Physics)*, *119*(10), 8046-8062. doi: 10.1002/2014JA019852
- Bortnik, J., Albert, J., Artemyev, A., Li, W., Jun, C.-W., Grach, V., & Demekhov, A. (2022). Amplitude dependence of nonlinear precipitation blocking of relativistic electrons by large amplitude EMIC waves. *Geophys. Res. Lett.*, submitted.
- Burch, J. L., Moore, T. E., Torbert, R. B., & Giles, B. L. (2016, March). Magnetospheric Multiscale Overview and Science Objectives. *Space Sci. Rev.*, *199*, 5-21. doi: 10.1007/s11214-015-0164-9
- Drozhdov, A. Y., Shprits, Y. Y., Usanova, M. E., Aseev, N. A., Kellerman, A. C., & Zhu, H. (2017, August). EMIC wave parameterization in the long-term VERB code simulation. *J. Geophys. Res.*, *122*, 8488-8501. doi: 10.1002/2017JA024389
- Drummond, W. E., & Pines, D. (1962). Nonlinear stability of plasma oscillations. *Nuclear Fusion Suppl.*, *3*, 1049-1058.
- Engebretson, M. J., Posch, J. L., Wygant, J. R., Kletzing, C. A., Lessard, M. R., Huang, C.-L., ... Shiokawa, K. (2015, July). Van Allen probes, NOAA, GOES, and ground observations of an intense EMIC wave event extending over 12 h in magnetic local time. *J. Geophys. Res.*, *120*, 5465-5488. doi: 10.1002/2015JA021227
- Ergun, R. E., Tucker, S., Westfall, J., Goodrich, K. A., Malaspina, D. M., Summers, D., ... Cully, C. M. (2016, March). The Axial Double Probe and Fields Signal Processing for the MMS Mission. *Space Sci. Rev.*, *199*, 167-188. doi: 10.1007/s11214-014-0115-x
- Fedorenko, Y., Tereshchenko, E., Pilgaev, S., Grigoryev, V., & Blagoveshchenskaya, N. (2014, December). Polarization of ELF waves generated during “beat-wave” heating experiment near cutoff frequency of the Earth-ionosphere waveguide. *Radio Science*, *49*(12), 1254-1264. doi: 10.1002/2013RS005336
- Glauert, S. A., & Horne, R. B. (2005, April). Calculation of pitch angle and energy diffusion coefficients with the PADIE code. *J. Geophys. Res.*, *110*, 4206. doi: 10.1029/2004JA010851
- Goldstein, J., de Pascuale, S., Kletzing, C., Kurth, W., Genestreti, K. J., Skoug, R. M., ... Spence, H. (2014, September). Simulation of Van Allen Probes plasmopause encounters. *J. Geophys. Res.*, *119*, 7464-7484. doi: 10.1002/2014JA020252
- Grach, V. S., & Demekhov, A. G. (2020, February). Precipitation of Relativistic Electrons Under Resonant Interaction With Electromagnetic Ion Cyclotron Wave Packets. *Journal of Geophysical Research (Space Physics)*, *125*(2), e27358. doi: 10.1029/2019JA027358
- Grach, V. S., Demekhov, A. G., & Larchenko, A. V. (2021, December). Resonant interaction of relativistic electrons with realistic electromagnetic ion-cyclotron wave packets. *Earth, Planets and Space*, *73*(1), 129. doi: 10.1186/s40623-021-01453-w
- Horwitz, J. L., Comfort, R. H., Richards, P. G., Chandler, M. O., Chappell, C. R., Anderson, P., ... Brace, L. H. (1990, June). Plasmasphere-ionosphere coupling 2. Ion composition measurements at plasmaspheric and ionospheric altitudes and comparison with modeling results. *J. Geophys. Res.*, *95*(A6), 7949-7959.

- doi: 10.1029/JA095iA06p07949
- Inan, U. S., Bell, T. F., & Helliwell, R. A. (1978, Jul). Nonlinear pitch angle scattering of energetic electrons by coherent VLF waves in the magnetosphere. *J. Geophys. Res.*, *83*(A7), 3235-3254. doi: 10.1029/JA083iA07p03235
- Karpman, V. I. (1974, September). Nonlinear Effects in the ELF Waves Propagating along the Magnetic Field in the Magnetosphere. *Space Sci. Rev.*, *16*, 361-388. doi: 10.1007/BF00171564
- Kennel, C. F., & Petschek, H. E. (1966, January). Limit on Stably Trapped Particle Fluxes. *J. Geophys. Res.*, *71*, 1-28.
- Kersten, T., Horne, R. B., Glauert, S. A., Meredith, N. P., Fraser, B. J., & Grew, R. S. (2014, November). Electron losses from the radiation belts caused by EMIC waves. *J. Geophys. Res.*, *119*, 8820-8837. doi: 10.1002/2014JA020366
- Kitahara, M., & Katoh, Y. (2019, Jul). Anomalous Trapping of Low Pitch Angle Electrons by Coherent Whistler Mode Waves. *J. Geophys. Res.*, *124*(7), 5568-5583. doi: 10.1029/2019JA026493
- Kubota, Y., & Omura, Y. (2017, Jan). Rapid precipitation of radiation belt electrons induced by EMIC rising tone emissions localized in longitude inside and outside the plasmopause. *Journal of Geophysical Research (Space Physics)*, *122*(1), 293-309. doi: 10.1002/2016JA023267
- Kubota, Y., Omura, Y., & Summers, D. (2015, Jun). Relativistic electron precipitation induced by EMIC-triggered emissions in a dipole magnetosphere. *Journal of Geophysical Research (Space Physics)*, *120*(6), 4384-4399. doi: 10.1002/2015JA021017
- Lindqvist, P.-A., Olsson, G., Torbert, R. B., King, B., Granoff, M., Rau, D., ... Tucker, S. (2016, March). The Spin-Plane Double Probe Electric Field Instrument for MMS. *Space Sci. Rev.*, *199*, 137-165. doi: 10.1007/s11214-014-0116-9
- Lundin, B. V., & Shkliar, D. R. (1977, October). Interaction of electrons with low transverse velocities with VLF waves in an inhomogeneous plasma. *Geomagnetism and Aeronomy*, *17*, 246-251.
- Ma, Q., Li, W., Thorne, R. M., Ni, B., Kletzing, C. A., Kurth, W. S., ... Angelopoulos, V. (2015, February). Modeling inward diffusion and slow decay of energetic electrons in the Earth's outer radiation belt. *Geophys. Res. Lett.*, *42*, 987-995. doi: 10.1002/2014GL062977
- Malaspina, D. M., Zhu, H., & Drozdov, A. Y. (2020, February). A Wave Model and Diffusion Coefficients for Plasmaspheric Hiss Parameterized by Plasmopause Location. *Journal of Geophysical Research (Space Physics)*, *125*(2), e27415. doi: 10.1029/2019JA027415
- Millan, R. M., & Baker, D. N. (2012, November). Acceleration of Particles to High Energies in Earth's Radiation Belts. *Space Sci. Rev.*, *173*, 103-131. doi: 10.1007/s11214-012-9941-x
- Mourenas, D., Artemyev, A. V., Zhang, X. J., Angelopoulos, V., Tsai, E., & Wilkins, C. (2021, November). Electron Lifetimes and Diffusion Rates Inferred From ELFIN Measurements at Low Altitude: First Results. *Journal of Geophysical Research (Space Physics)*, *126*(11), e29757. doi: 10.1029/2021JA029757
- Ni, B., Cao, X., Zou, Z., Zhou, C., Gu, X., Bortnik, J., ... Xie, L. (2015, September). Resonant scattering of outer zone relativistic electrons by multiband EMIC waves and resultant electron loss time scales. *J. Geophys. Res.*, *120*, 7357-7373. doi: 10.1002/2015JA021466
- Omura, Y., Matsumoto, H., Nunn, D., & Rycroft, M. J. (1991, May). A review of observational, theoretical and numerical studies of VLF triggered emissions. *Journal of Atmospheric and Terrestrial Physics*, *53*, 351-368.
- Omura, Y., & Zhao, Q. (2013, August). Relativistic electron microbursts due to nonlinear pitch angle scattering by EMIC triggered emissions. *J. Geophys.*

- Res.*, 118, 5008-5020. doi: 10.1002/jgra.50477
- Shklyar, D. R., & Matsumoto, H. (2009, April). Oblique Whistler-Mode Waves in the Inhomogeneous Magnetospheric Plasma: Resonant Interactions with Energetic Charged Particles. *Surveys in Geophysics*, 30, 55-104. doi: 10.1007/s10712-009-9061-7
- Shprits, Y. Y., Drozdov, A. Y., Spasojevic, M., Kellerman, A. C., Usanova, M. E., Engebretson, M. J., ... Aseev, N. A. (2016, September). Wave-induced loss of ultra-relativistic electrons in the Van Allen radiation belts. *Nature Communications*, 7, 12883. doi: 10.1038/ncomms12883
- Shprits, Y. Y., Elkington, S. R., Meredith, N. P., & Subbotin, D. A. (2008, November). Review of modeling of losses and sources of relativistic electrons in the outer radiation belt I: Radial transport. *Journal of Atmospheric and Solar-Terrestrial Physics*, 70, 1679-1693. doi: 10.1016/j.jastp.2008.06.008
- Shprits, Y. Y., Kellerman, A., Aseev, N., Drozdov, A. Y., & Michaelis, I. (2017, Feb). Multi-MeV electron loss in the heart of the radiation belts. *Geophys. Res. Lett.*, 44(3), 1204-1209. doi: 10.1002/2016GL072258
- Shprits, Y. Y., Subbotin, D. A., Meredith, N. P., & Elkington, S. R. (2008, November). Review of modeling of losses and sources of relativistic electrons in the outer radiation belt II: Local acceleration and loss. *Journal of Atmospheric and Solar-Terrestrial Physics*, 70, 1694-1713. doi: 10.1016/j.jastp.2008.06.014
- Summers, D. (2005, August). Quasi-linear diffusion coefficients for field-aligned electromagnetic waves with applications to the magnetosphere. *J. Geophys. Res.*, 110, 8213. doi: 10.1029/2005JA011159
- Summers, D., Ni, B., & Meredith, N. P. (2007, April). Timescales for radiation belt electron acceleration and loss due to resonant wave-particle interactions: 2. Evaluation for VLF chorus, ELF hiss, and electromagnetic ion cyclotron waves. *J. Geophys. Res.*, 112, 4207. doi: 10.1029/2006JA011993
- Summers, D., & Thorne, R. M. (2003, April). Relativistic electron pitch-angle scattering by electromagnetic ion cyclotron waves during geomagnetic storms. *J. Geophys. Res.*, 108, 1143. doi: 10.1029/2002JA009489
- Thorne, R. M., & Kennel, C. F. (1971). Relativistic electron precipitation during magnetic storm main phase. *J. Geophys. Res.*, 76, 4446. doi: 10.1029/JA076i019p04446
- Torkar, K., Nakamura, R., Tajmar, M., Scharlemann, C., Jeszenszky, H., Laky, G., ... Svenes, K. (2014, May). Active Spacecraft Potential Control Investigation. *Space Sci. Rev.* . doi: 10.1007/s11214-014-0049-3
- Tsyganenko, N. A. (1989, January). A magnetospheric magnetic field model with a warped tail current sheet. *Planetary Space Science*, 37, 5-20. doi: 10.1016/0032-0633(89)90066-4
- Usanova, M. E., Drozdov, A., Orlova, K., Mann, I. R., Shprits, Y., Robertson, M. T., ... Wygant, J. (2014, March). Effect of EMIC waves on relativistic and ultrarelativistic electron populations: Ground-based and Van Allen Probes observations. *Geophys. Res. Lett.*, 41, 1375-1381. doi: 10.1002/2013GL059024
- Vedenov, A. A., Velikhov, E., & Sagdeev, R. (1962). Quasilinear theory of plasma oscillations. *Nuclear Fusion Suppl.*, 2, 465-475.
- Wang, G., Su, Z., Zheng, H., Wang, Y., Zhang, M., & Wang, S. (2017). Nonlinear fundamental and harmonic cyclotron resonant scattering of radiation belt ultrarelativistic electrons by oblique monochromatic emic waves. *J. Geophys. Res.*, 122(2), 1928-1945. Retrieved from <http://dx.doi.org/10.1002/2016JA023451> doi: 10.1002/2016JA023451
- Zhu, H., Chen, L., Claudepierre, S. G., & Zheng, L. (2020, February). Direct Evidence of the Pitch Angle Scattering of Relativistic Electrons Induced by EMIC Waves. *Geophys. Res. Lett.*, 47(4), e85637. doi: 10.1029/2019GL085637